JOURNAL OF CATALYSIS 73, 272–287 (1982)

# Adsorption–Desorption Kinetics of $H_2$ from Supported Nickel Catalysts

P. I. LEE AND J. A. SCHWARZ

*Department of Chemical Engineering and Materials Science, Syracuse University, Syracuse, New York 13210*

Received July 14, 1981; revised September 30, 1981

The adsorption–desorption interactions of hydrogen from a nickel-supported silica catalyst were studied by pulsed chemisorption and temperature-programmed desorption (TPD) techniques incorporating on-line mass spectrometric detection in a flow system. Pulsed chemisorption results of the metal surface area agree with results from more conventional static measurements. A combination of pressure pulse analysis and flow rate variation allowed the adsorption kinetics to be determined as $(1 - \theta)^2$, where $\theta$ is the fractional coverage. The activation energy for adsorption, $E_a$, is nearly zero. TPD spectra showed a general trend of second-order desorption kinetics with a shift in peak temperature to lower temperatures as the coverage was increased. After experimentally eliminating all transport considerations which would have caused shaping of the spectra, a self-consistent analysis of the desorption rate isotherms, characteristic plots, and lineshapes of the spectra led to the conclusion that free readsorption of hydrogen dominated during the desorption. The activation energy, $E_d$, is 89 kJ/mole at low coverage and 55 kJ/mole at higher coverages. The falloff in $E_d$ with $\theta$ occurs at a critical coverage which is strongly dependent on the sample weight. When the role of readsorption was clarified and provided that the catalyst bed length approached "differential bed" requirements, the variation in the activation energy with coverage agreed quantitatively with results obtained from single-crystal experiments. The compensation effect in the desorption rate constant was also observed.

## INTRODUCTION

The technique of temperature-programmed desorption (TPD) was originally applied to oxide catalysts to yield information on binding energies and reaction sites (*1*). More recently this technique has been used to study the desorption process from supported metal catalysts (*2, 3*). Although an extensive theoretical description exists for interpreting TPD spectra, the majority of the recent studies have been limited to qualitative analyses of desorption data. This approach has yielded useful information especially with regard to studying differences in catalysts due to metal used, preparation procedures, type of support, the presence of promoters, and the dispersion of the metal. However, detailed kinetic information such as the coverage dependence of binding energies of adsorbates has been lacking. In addition, the experimental apparatus used to perform TPD experiments can readily be employed to study the adsorption kinetics of gases; no such studies have been reported. It is apparent the full utility of the TPD technique has not been exploited in the studies to date.

A basis for comparison and evaluation of the kinetic data obtained from the TPD technique can be found in the results of adsorption–desorption of gases from single crystals performed under the well-controlled conditions afforded by ultrahigh vacuum. Our studies have been directed at examining to what extent adsorption–desorption data from supported metal catalysts at atmospheric pressure can be correlated with similar data obtained from their unsupported metal analogs.

Here we report on a pulsed chemisorption technique combined with the TPD method to study the adsorption–desorption kinetics of hydrogen from a nickel sup-



0021-9517/82/020272-16$02.00/0

ported on silica catalyst. Both practical and fundamental considerations dictated the choice of this catalyst. Practically, we were fortunate to obtain this catalyst from J. L. Carter of Exxon Research and Engineering. A complete physical characterization was available. From a more fundamental concern we wished to minimize any support–metal interactions that are known to occur for other catalyst systems. The hope was that the body of data available from single-crystal studies of hydrogen interaction with nickel might be helpful in our interpretation of the data.

In the sections to follow we will first describe the methods for analysis of pulsed chemisorption and TPD data, respectively. A theoretical description of the adsorption–desorption process germane to the hydrogen/nickel system will be presented. A description of the experimental apparatus will then be given. We use continuous mass spectrometric analysis of the effluent stream below a differential flow reactor configuration. The adsorption–desorption results of hydrogen from the supported nickel catalyst will then be presented. The pulsed adsorption experiments and the variation of uptake with flow rate have enabled us to determine the adsorption kinetics, the metal surface area, and the initial sticking coefficient of hydrogen. The desorption kinetics will be reduced to a semiquantitative description of the variation of the activation energy for desorption of hydrogen as a function of its coverage. We will then discuss these results by comparing them with the single-crystal data (*4–6*) and data obtained by Padberg and Smith (*7*) from supported nickel using a chromatographic technique.

## DATA ANALYSIS

### A. *Background*

Pulsed chemisorption studies have been employed to determine metal surface areas (*8, 9*) and kinetic processes following adsorption (*10, 11*). For the latter case, both reversible and irreversible reactions have been considered (*11*). Analyses of irreversible reactions with zero-, first-, and second-order kinetics have been made for the case of rectangular or triangular pulses of reactants (*10*). These results have been applied to, for example, studies of the dehydrogenation of cyclohexane on several catalysts. We will show that the combination of pulsed chemisorption followed by TPD can also be used to determine the adsorption kinetics.

In most TPD experiments, only a small fraction of the data obtained is used in the desorption kinetic analysis. Usually the temperature of the peak maximum is noted and its temperature variation with initial coverage is used to qualitatively identify the order of the desorption (*12, 13*).

The desorption rate isothermal method (*14–18*) of data reduction utilizes more of the desorption data than a single point by examining a series of desorption curves obtained at different initial surface coverages. Under certain conditions, these spectra may be used directly to obtain desorption rates and coverages at selected temperatures in the desorption range. Implicit in this analysis is the requirement that the coverage at a specified temperature in the desorption range is simply the area under the TPD spectrum from that temperature to a temperature sufficiently high enough that no desorption is occurring. If readsorption occurs freely, for example, then the data must be carefully analyzed when the desorption rate isothermal method is used. We will discuss this situation in detail later. When no readsorption occurs, each isotherm becomes a characteristic plot of ln(Rate) vs ln(Coverage) measured at a given temperature and its slope corresponds to the order of the desorption. One might expect that over a certain range of coverages this order would correspond to expected values of, for example, one for a first order desorption or two for second-order desorption. When the activation energy changes with coverage, the "appar-

ent'' order of the desorption changes. From a series of desorption rate isotherms, plots of ln(Rate) against $T^{-1}$ can be obtained at fixed coverage and the activation energy can be determined at that coverage.

When transport processes or readsorption might be important the direct analysis of the data is not straightforward. Cvetanović and Amenomiya have considered these processes when the desorption was first order (*1*). Konvalinka *et al.* (*19*) have made a direct extension of the original analysis to second-order desorption processes. In both cases the complexity of the mathematical problem was reduced by the assumption that true differential bed conditions were met. Furthermore, the coverage dependence of the kinetic parameters was not considered. With these restrictions, the characteristic plot approach and lineshape analysis criterion were established. Desorption rate isothermal analysis can consider directly the coverage dependence of the kinetic parameters. However, no such analysis has been presented to our knowledge.

### *B. Adsorption*

The amount of uptake of an adsorbate pulse when it passes through a catalyst bed depends on several factors. These include the time-dependent partial-pressure distribution within the pulse, the contact time with the bed, and the adsorption temperature. The first two factors are determined by the carrier gas flow rate, the amount of adsorbate introduced, and the shape of the adsorbate pulse. If the amount of adsorbate in one single injected pulse is maintained constant, these factors should then depend only on the carrier gas flow rate. The amount of uptake as a function of flow rate enables a determination of the adsorption kinetics which will be shown as follows. To a good approximation, the pulses that we generate are triangular. Two parameters, intensity ($I$) and width ($W$), can be used to describe these pulses, $C(t)$ (*10*). The functional description of $C(t)$ is

$$\begin{aligned} C(t) &= 0, && t < 0, \\ &= \frac{2I}{W} ut, && 0 < t < \frac{W}{2u}, \\ &= \frac{2I}{W}(W - ut), && \frac{W}{2u} < t < \frac{W}{u}, \\ &= 0, && \frac{W}{u} < t, \end{aligned} \qquad (1)$$

where $u$ is the velocity of the carrier gas. Table 1 shows some experimental values of $u \int_0^\infty C(t)dt$ at different flow rates when the amount of adsorbate per injection was constant.

When a pulse is passed through the catalyst, both the amount of breakthrough and adsorbed can be measured mass spectrometrically. A mass balance between these quantities will give the degree of conversion, $\theta_t$, which is defined as the fraction of surface occupied by adsorbate and thus has the same meaning as the fractional coverage.

Desorption of hydrogen from the nickel surface will be shown to follow second-order desorption kinetics in a later section. This is consistent with the results from single-crystal data (*4–6*). However, both first-order (*4, 20*) and second-order (*5, 6, 21*) adsorption kinetics have been reported for the adsorption process. Considering both of these possibilities, mass balances on the surface phase may be written as

First-order adsorption:

$$-\frac{\partial\theta}{\partial t} = -k_a C(1 - \theta) + k_d\theta^2, \qquad (2a)$$

Second-order adsorption:

$$-\frac{\partial\theta}{\partial t} = -k_a C(1 - \theta)^2 + k_d\theta^2, \qquad (2b)$$

where $\theta$ is the fractional coverage of the surface phase, $C$ is the fluid phase concentration, and $k_a$, $k_d$ are rate constants for adsorption and desorption, respectively. These equations have been based on the assumption of a differential bed. This assumption was found to be reasonable for the adsorption process. However, for the

TABLE 1

Triangular Pulse Characteristics

| Flow rate ($cm^3$/min) | $I$ (intensity) (Arb. unit) | $W^*$ (Arb. unit) | $u\int_0^\infty C(t)dt = \frac{W^* \times I}{2}$ |
|---|---|---|---|
| 80 | 50.0 | 4.5 | 112.5 |
| 180 | 49.5 | 4.4 | 108.9 |
| 240 | 50.5 | 4.5 | 113.6 |
| 350 | 50.0 | 4.5 | 112.5 |

*Note.* $W^*$ is the width of the pulse normalized to the highest flow rate.

desorption process, such a condition is not valid. This point will be discussed shortly.

The desorption of hydrogen at room temperature is negligible over the experimental time scale; thus Eqs. (2a) and (2b) can be rewritten as

$$\frac{\partial\theta}{\partial t} = k_a C(1-\theta), \tag{3a}$$

$$\frac{\partial\theta}{\partial t} = k_a C(1-\theta)^2. \tag{3b}$$

We can rearrange and integrate Eqs. (3a) and (3b) as

$$\int_0^{\theta_f} \frac{d\theta}{1-\theta} = k_a \int_0^\infty C dt, \tag{4a}$$

$$\int_0^{\theta_f} \frac{d\theta}{(1-\theta)^2} = k_a \int_0^\infty C dt. \tag{4b}$$

The integral $u\int_0^\infty Cdt$, as shown in Table 1, is constant for different carrier gas flow rates if the amount of adsorbate injected remains constant. For first- or second-order adsorption kinetics, Eqs. (4a) and (4b) become

$$\ln(1-\theta_f)^{-1} \sim \nu_a e^{-E_a/RT} u^{-1}, \tag{5a}$$

$$\frac{\theta_f}{1-\theta_f} \sim \nu_a e^{-E_a/RT} u^{-1}. \tag{5b}$$

Here we have written the adsorption rate constant, $k_a$, in an Arrhenius form. The degree of conversion ($\theta_f$) as a function of flow velocity $u$ can be measured experimentally and thus the order of the adsorption process may be determined. The above equations can then be utilized to find the activation energy for adsorption by changing the adsorption temperature.

### C. Desorption

In analyzing TPD data, two equations need to be considered:

$$u\frac{\partial C}{\partial z} = -V_m \frac{\partial\theta}{\partial t}, \tag{6}$$

$$-\frac{\partial\theta}{\partial t} = -k_a C(1-\theta)^n + k_d\theta^p, \tag{7}$$

where $V_m$ is the number of surface sites per unit solid volume and $z$ is a length coordinate.

Further reduction of these equations can be made by invoking true differential bed conditions. Here the carrier gas flows through a uniformly packed catalyst bed and the bed itself is very shallow, so that the concentration of the adsorbate in the gas phase at any time is to a good approximation uniform throughout the catalyst bed. Others have examined the case of free readsorption when $p = 1$ (*4, 20*) and $p = 2$ (*5, 6, 21*), but have assumed that true differential bed conditions exist. If during desorption, free readsorption is a major consideration, the effect is to "hold" the adsorbate in the bed longer than would be expected even if the bed thickness were short enough that differential bed behavior would normally be expected. The minimum bed thickness for true differential bed behavior depends on the extent that readsorption dominates the overall desorption process. We can still simplify Eqs. (6) and (7) if we keep this fact in mind when examining the data. We would expect that the smaller the bed thickness and the lower the coverage of adsorbate true differential bed character would be attained. This important point will be discussed later.

For a true differential bed of $V_m$ surface sites per unit solid volume, and $V_c$ total solid volume Eqs. (6) and (7) become

$$-\frac{d\theta}{dt} = k_d(\theta)\theta^p - k_a C(1-\theta)^n, \tag{8}$$

$$FC = V_c V_m k_d(\theta)\theta^p - V_c V_m k_a C(1-\theta)^n. \quad (9)$$

As developed by others, these equations are the usual starting point for analysis (*1*). Since the coverage dependence of the kinetic parameters is of interest, we will proceed to develop these equations into a form such that characteristic plots for desorption rate isothermal analysis may be employed. Recall, this approach makes no assumption about the form of the coverage dependence of the kinetic parameters.

The concentration of the fluid phase, $C$, is obtained from Eq. (9)

$$C = \frac{V_c V_m k_d(\theta)\theta^p}{F + V_c V_m k_a (1-\theta)^n}. \quad (10)$$

If a linear temperature-programming rate is used

$$T(t) = T_0 + \beta t. \quad (11)$$

A combination of Eqs. (8), (9), and (11) yields

$$C = -\frac{V_c V_m \beta}{F}\frac{d\theta}{dT}. \quad (12)$$

In Eq. (12), $d\theta/dT$ is the desorption rate of the surface phase and is proportional to the fluid concentration eventually detected.

Anticipating our future discussions we will consider Eq. (12) under the limiting case of dissociative mobile adsorption ($n = 2$) and for second-order desorption kinetics ($p = 2$). When readsorption is small $F \gg V_c V_m k_a (1-\theta)^2$. Equations (10) and (12) can be written as

$$-\frac{d\theta}{dT} = \frac{k_d(\theta)}{\beta}\theta^2. \quad (13a)$$

When readsorption occurs freely $F \ll V_c V_m k_a (1-\theta)^2$ and Eqs. (10) and (12) become

$$-\frac{d\theta}{dT} = \frac{F}{V_c V_m \beta}\frac{k_d(\theta)}{k_a}\left(\frac{\theta}{1-\theta}\right)^2. \quad (13b)$$

If an Arrhenius form for the rate constant is adopted, then Eqs. (13a) and (13b) can be written as

$$-\frac{d\theta}{dT} = \frac{\nu_d(\theta)}{\beta} e^{-E_d(\theta)/RT}\theta^2, \quad (14a)$$

$$-\frac{d\theta}{dT} = \frac{F}{V_c V_m \beta}\frac{\nu_d(\theta)}{\nu_a} e^{-\Delta H(\theta)/RT}\left(\frac{\theta}{1-\theta}\right)^2. \quad (14b)$$

Here the activation energy and preexponential factor for desorption have been expressed as a function of coverage and $\Delta H = E_d - E_a$. If a series of TPD spectra is obtained for different initial coverages at constant heating rate and constant carrier gas flow rate, either (14a) or (14b) may be used to obtain the coverage dependence of the kinetic parameters by using the desorption rate isothermal analysis.

On the other hand, if $E_d$ and $\nu_d$ are independent of coverage, Eqs. (14a) and (14b) can be treated by the single-point peak temperature analysis previously described to give

$$\ln(\theta_m T_m^2) = \ln\beta + \frac{E_d}{RT_m} + \ln\left(\frac{F}{2\nu_d R}\right), \quad (15a)$$

$$\ln\left(\frac{\theta_m T_m^2}{(1-\theta_m)^3}\right) = \ln\beta + \frac{\Delta H}{RT_m} + \ln\left(\frac{V_c V_m \nu_a \Delta H}{2FR\nu_d}\right). \quad (15b)$$

Again, if a series of TPD spectra is obtained for different initial coverages at constant heating rate and constant carrier gas flow rate, the kinetic parameters can be derived from characteristic plots of $\ln(\theta_m T_m^2)$ vs $1/T_m$ or $\ln(\theta_m T_m^2)/(1-\theta_m)^3$ vs $1/T_m$ for the cases of no readsorption and when readsorption dominates, respectively.

Our results will be analyzed on the basis of Eqs. (5a) and (5b) for adsorption and Eqs. (14a), (14b), (15a), and (15b) for desorption. We state again these equations are valid only when true differential bed conditions are met. The deviation from this condition will be clearly indicated in our analysis. The details of our experimental apparatus and procedures will be described before presenting our results.

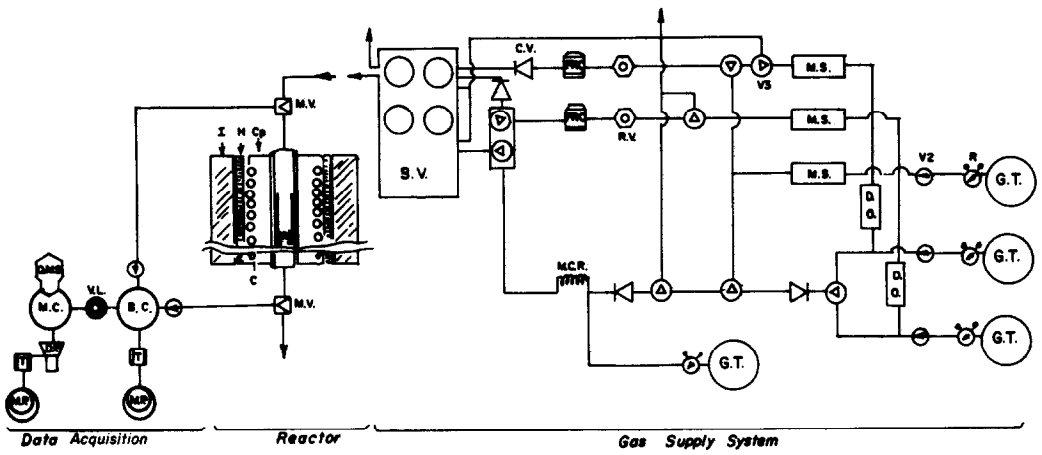


B.C. = Buffer Chamber
C = Cooling Coil
Cp = Copper Shell
C.V. = Check Valve
D.O. = Deoxy Unit
D.P. = Diffusion Pump
F.R.C. = Flow Rate Controller
G.T. = Gas Tank
H = Heating Element
I = Insulation Material
M.C.R. = Metal Carbonyl Remover
M.C. = Main Vacuum Chamber
M.P. = Mechanical Pump
M.S. = Molecular Sieve
M.V. = Metering Valve
Q.M.S = Quadrupole Mass Spectrometer
R = Regulator
R.V. = Relief Valve
S.V. = Sample Valve
T = Trap
V2 = Two Way Valve
V3 = Three Way Valve
V.L. = Variable Leak Valve

FIG. 1. Schematic of gas supply system, reactor, and data acquisition system.

## EXPERIMENTAL

The differential flow reactor system in which the adsorption–desorption studies were performed is shown schematically in Fig. 1. The essential features of this equipment are an automatic switching valve to provide injection of known amounts of adsorbate into a helium carrier gas stream and a quadrupole mass spectrometer which enables a continuous monitoring of the gas-phase effluent from the reactor.

Extensive details of the construction of the apparatus may be found elsewhere (*22*). Here we will describe briefly the various elements which make up the overall flow and detection system.

### *A. Gases*

The ultrahigh-purity-grade hydrogen (99.999%) came from Linde Division, Union Carbide, and was further purified by processing through a bed of an oxidation catalyst (Scientific Gas Products) and a bed of molecular sieve (Linde). The scientific-grade helium (99.9999%) from M. G. Scientific Gas was further purified by a bed of molecular sieve. Both gases were mass spectroscopically checked to be moisture free. The oxygen content, estimated to be less than 0.5 ppm, did not contaminate the catalyst after continuous experiments for 30 h.

### *B. Catalyst*

The nickel on silica catalyst was supplied by J. L. Carter, Exxon Research and Engi-

TABLE 2

Properties of the Catalyst

| | |
|---|---|
| Nickel content | ~45–49 wt% |
| Apparent particle density | $\rho_p$ = 1.57–1.61 g/cm³ catalyst |
| Porosity | $\beta$ = ~0.30–0.38 cm³/g catalyst |
| Nickel surface area | ~70–80 m²/g catalyst |
| Total surface area (BET) | ~270–290 m²/g catalyst |
| Average crystallite size | 20–22 Å |

TABLE 3

Bed Characteristics

| Bed No. | Mass of catalyst (g) | Bed void fraction | Bed length (mm) | Particle size (mm) |
|---|---|---|---|---|
| I | 0.200 | 0.55 | 10.0 | 0.225 |
| II | 0.100 | 0.54 | 5.0 | 0.225 |
| III | 0.022 | 0.55 | 2.0 | 0.225 |
| IV | 0.100 | ~0.35–0.40 | 4.5 | 0.025 |

neering. The nickel content in the catalyst, after calcination and before reduction, is from 45 to 49 wt%. The metal surface area, determined by hydrogen chemisorption, ranges from 70 to 80 $m^2/g$ catalyst. The total surface area measured by the BET method varies between 270 to 290 $m^2/g$ catalyst. The porosity is 0.3 to 0.38 $cm^3/g$ catalyst. The nickel crystallite size which ranges between 20 and 22 Å was determined by X-ray line broadening measurement before the catalyst was reduced. These properties of the catalyst are summarized in Table 2.

Catalysts of varying particle size were prepared by grinding. The resulting particles are size-graded with nylon sieve cloth of mesh numbers between 50 and 100 (0.149 to 0.297 mm). Particles of size smaller than 400 mesh (0.038 mm) were collected beneath a stainless-steel sieve cloth. Their size was estimated by optical microscopy and proved to be predominantly within 0.015 to 0.038 mm.

During the course of these studies we found that even for a catalyst charge of less than 0.022 g, the true differential character of the reactor is not met over the range of experimental variables. Thus the properties of the catalyst beds formed from the catalyst described in Table 2 are important and are presented in Table 3. We will discuss this point in more detail later.

### *C. Reactor and Gas Injection System*

The tubular reactor is made of stainless

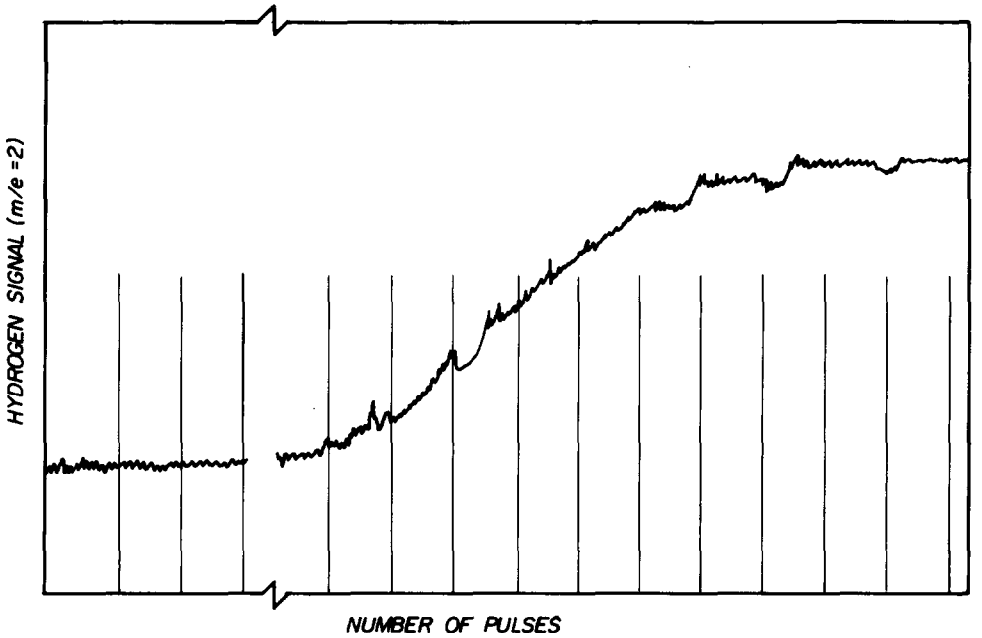


FIG. 2. Mass spectrometer trace of $H_2$ peak during pulsed chemisorption. Each vertical line denotes injection of $2.5 \times 10^{-2}$ $cm^3$ of sample gas into the carrier stream where bulk velocity was 20 $cm^3$/min. Note that no increase in the $H_2$ signal is seen until after ~80 pulses (see text).

steel. The reactor consists of an outer shell with a small microreactor insert. The tubular shell is 15.2 cm long with an o.d. of 0.952 cm and an i.d. of 0.714 cm. The ground, weighed, and size-graded catalyst is placed in the microreactor which is 20 mm long, 7.14 mm o.d., and 5.95 mm i.d. The microreactor has a 400-mesh stainless-steel wire cloth at the bottom to prevent loss of catalyst. Particles of size smaller than 400 mesh are supported by a quartz fritted disk (Corning No. 39570). The microreactor sits on a ring platform inside the tubular shell.

A Cajon VCR fitting is connected to each end of the stainless-steel shell and sealed with copper gaskets. The shell is surrounded by two semicylindrical copper shells. These shells provide excellent heat conduction and result in a uniform temperature distribution throughout the microreactor insert. In order to provide input signals to a temperature controller, a stainless-steel sheathed iron–constantan thermocouple with an ungrounded tip is placed into the copper shell. Another stainless-steel sheathed Chromel–Alumel thermocouple is inserted into the catalyst bed via a Swagelok feed-thru for the measurement of the bed temperature. A 0.318-cm copper tube with cooling water is wrapped along a helical trail machined on the copper shell surface. The reactor setup fits into an oven with two semicylindrical Nichrome heating units with a maximum power output of 600 W. The temperature can be controlled by a temperature programmer (Hewlett–Packard, F & M Scientific 240) at rates from 0.5 to 30°C/min.

Gases supplied to the reactor are first regulated by two-stage regulators, and then controlled by Tylan flow controllers. The

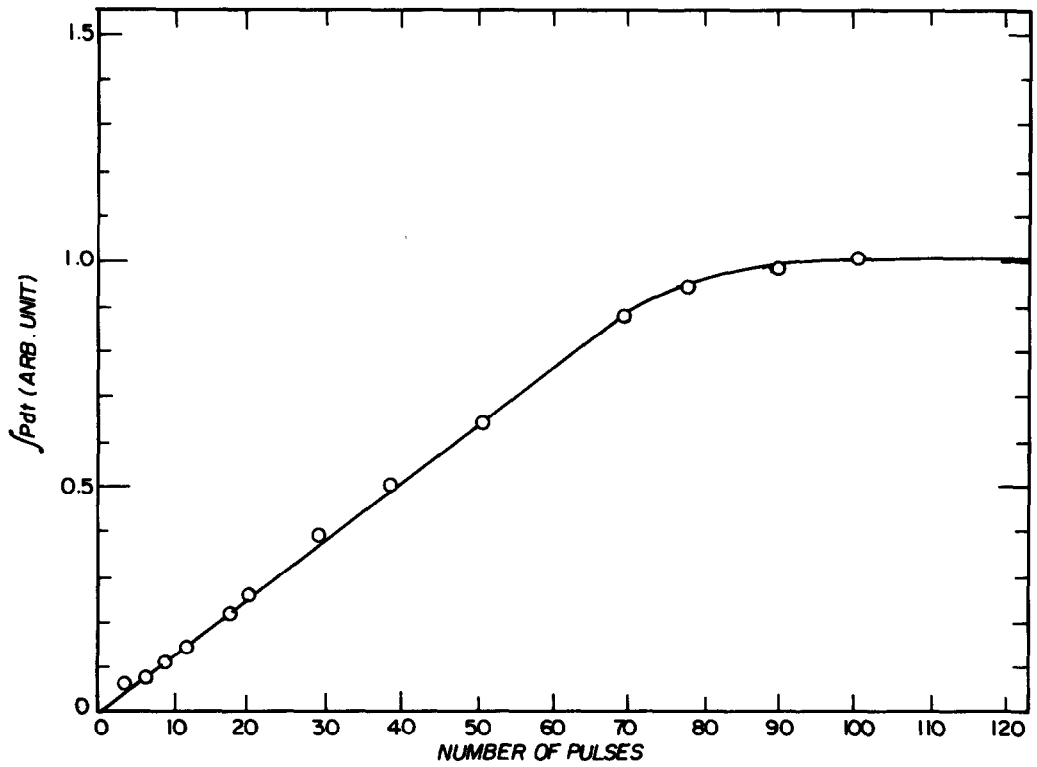


FIG. 3. Pulse-wise hydrogen chemisorption at 290°K. $\int Pdt$ is the area under the corresponding TPD spectra.

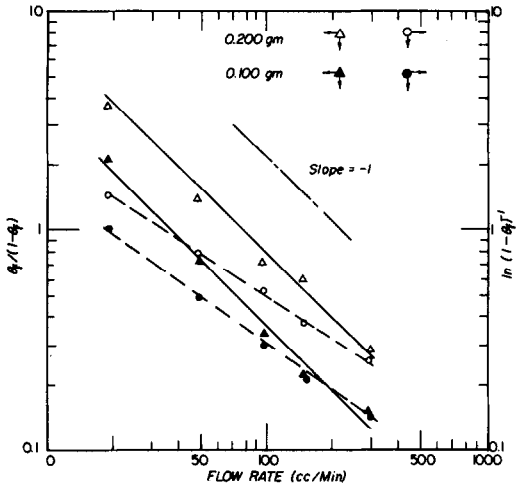


FIG. 4. Test of first-order and second-order rate laws for hydrogen chemisorption at 290°K for sample weights of 0.200 and 0.100 g, respectively. Second-order rate law yields best straight line with slope −1.

sampling valve device, controlled by a Valco valve sequence programmer, permits injection of either square-wave or triangular-wave samples of different volume ($5 \times 10^{-4}$ cm³ to infinity). The shapes of these pulses are determined by the carrier gas flow rate. During experiments, the sampling valve is kept at 80°C, and the downstream flow lines are maintained at temperatures of 70–80°C by heating tapes in order to minimize wall effects.

### D. Detection System

A Varian VGA-100 quadrupole mass spectrometer is used to analyze the composition of the gas effluent from the catalyst bed. The base pressure within this portion of the system is typically $5 \times 10^{-9}$ Torr (1 Torr = 133.3 N/m²) and is maintained by a 2-in. cold trapped oil diffusion pump. Atmospheric pressure sampling is first accomplished by Swagelok cross-pattern valves (SS-4MX) located directly above and below the Cajon VCR fittings. Sampled gas is directed to a buffer chamber where pressure is controlled by a throttling valve at 100 mTorr. The buffer chamber is pumped by a Welch mechanical pump that is trapped with a bakeable molecular sieve trap. All traps are routinely baked. Final gas inlet to the mass spectrometer is accomplished by a Varian variable leak valve. The mass spectrometer chamber pressure is maintained at $10^{-6}$ Torr during experiments.

### E. Procedures

The fresh catalyst is first dehydrated in a helium flow (50 cm³/min) at temperatures of 485°C for 2 h. The reactor is then cooled to room temperature by introducing cooling water. The flow is switched from helium to hydrogen and the temperature is slowly increased to 485°C where it is maintained for 3 h. During this temperature-programmed reduction the *m/e* 18 peak is continuously monitored. The spectra show two major peaks at 90 and 200°C and a small peak at 450°C, which are reproducible from experiment to experiment. When the reduction is completed, the gas flow is switched back to helium and the reactor is cooled to room temperature. Samples of hydrogen of known amount are injected into the helium carrier gas at flow rates ranging from 20 to 300 cm³/min depending on the experiment. The amount of breakthrough is measured mass spectroscopically. After this pulsed adsorption procedure the adsorbate is ther-

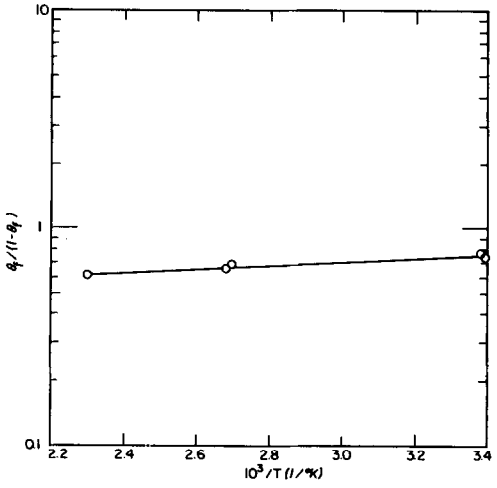


FIG. 5. Adsorption energy determination of $H_2$ on $Ni/SiO_2$ following second-order rate law.

mally desorbed. Typical TPD spectra are obtained at heating rates of 30°C/min and helium flow rates of 100 cm³/min. A very high activity for hydrogen chemisorption is observed on the first few TPD spectra collected right after reduction. However, the activity of the catalyst becomes stable in succeeding experiments as indicated by the reproducibility of our results.

## RESULTS

### A. *Adsorption*

Figure 2 shows a mass spectrometer trace of the hydrogen peak as a function of the time sampled from the effluent of the carrier gas below the differential flow reactor. The catalyst charge was 0.100 g and the flow velocity was 20 cm³/min. The catalyst was maintained at room temperature. The vertical spikes are generated from the trigger of the programmer which activates the switching valve. Each spike indicates the injection of 0.025 cm³ of hydrogen into the helium stream. Breakthrough occurred after 80 pulses or 2.0 cm³ of hydrogen. The adsorption stoichiometry has been shown to be H/Ni = 1 (*23*, *24*). If we assume uniform adsorption and an area for H of 6.8 × $10^{-2}$ nm²/atom (*23*), then the metal surface area is calculated to be 60 m²/g. This is in good agreement with the static hydrogen chemisorption data supplied by Carter.

In Fig. 3 the areas under the TPD peak after pulsed adsorption sequences are shown as a function of the number of pre-

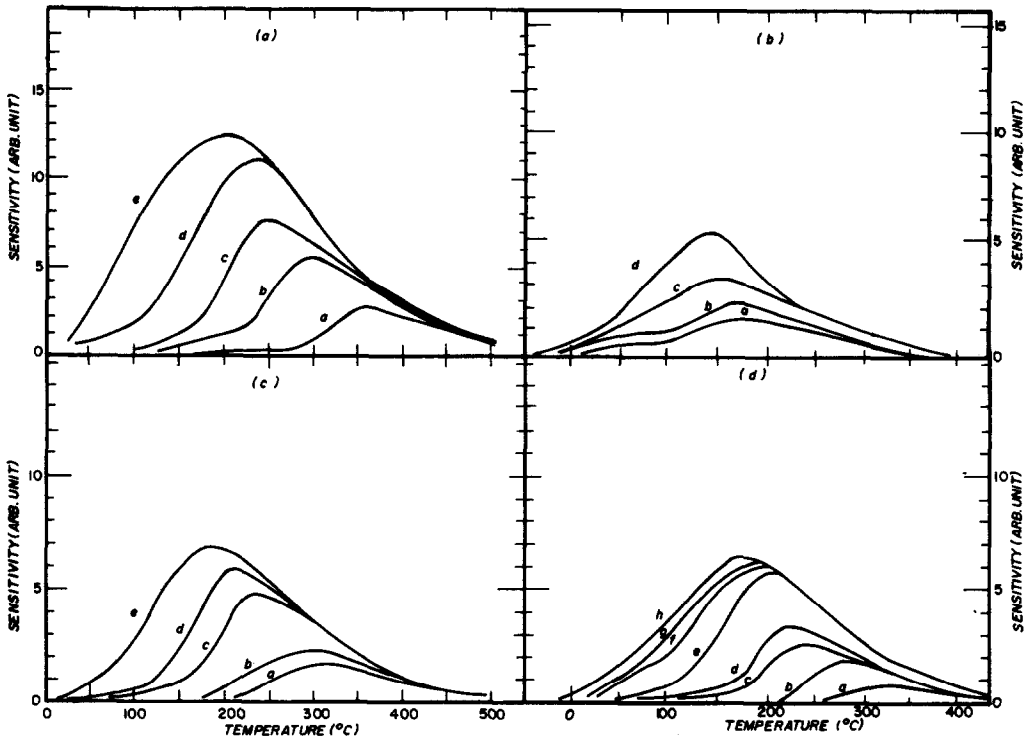


FIG. 6. TPD spectra for $H_2$ after adsorption at 295°K. Heating rate, 30°C/min; flow rate 100 cm³/min. (a) Sample weight = 0.200 g, $D_p$ = 225 μm. Coverages indicated on figure are (a) $\theta$ = 0.12, (b) $\theta$ = 0.32, (c) $\theta$ = 0.48, (d) $\theta$ = 0.76, (e) $\theta$ = 1.00. (b) Sample weight = 0.022 g, $D_p$ = 225 μm. Coverages indicated on figure are (a) $\theta$ = 0.30, (b) $\theta$ = 0.44, (c) $\theta$ = 0.68, (d) $\theta$ = 1.00. (c) Sample weight = 0.100 g, $D_p$ = 225 μm. Coverages indicated on figure are (a) $\theta$ = 0.15, (b) $\theta$ = 0.20, (c) $\theta$ = 0.61, (d) $\theta$ = 0.70, (e) $\theta$ = 1.00. (d) Sample weight = 0.100 g, $D_p$ = 25 μm. Coverages indicated on figure are (a) $\theta$ = 0.05, (b) $\theta$ = 0.16, (c) $\theta$ = 0.25, (d) $\theta$ = 0.34, (e) $\theta$ = 0.72, (f) $\theta$ = 0.83, (g) $\theta$ = 0.90, (h) $\theta$ = 1.00.

vious pulses. The initial rise is linear. The amount adsorbed saturates after 80 pulses in agreement with the conclusion one may infer from Fig. 2. The initial slope is $1.5 \times 10^{13}$ molecules/cm$^2$ pulse. It will be shown later that from this data we may estimate the initial sticking coefficient of hydrogen on nickel.

The amount adsorbed as a function of flow rate in one single injected pulse enables us to determine the adsorption kinetics. Two models have been considered and the characteristic plots are suggested by Eqs. (5a) and (5b). Data at room temperature are shown in Fig. 4 for the two cases considered. Clearly the best straight lines with slope $-1$ are obtained for dissociative mobile adsorption, i.e., $(1 - \theta)^2$ kinetics. The temperature dependence of the adsorption rate constant (Eq. (5b)) is shown in Fig. 5. The slope is essentially zero which confirms earlier results (*21, 25*).

### *B. Desorption*

Figures 6a–d show TPD spectra for catalyst samples of different weight and different particle size. The variation in initial coverages is small and controlled by the method described previously. The temperature-programmed desorption is carried out at constant heating rate and constant carrier gas flow rate. The general trend of a peak temperature shift to higher temperature as the initial coverage decreases is observed. The shift in peak temperature is found to be independent of the particle size. This eliminates the possibility of intraparticle diffusion control. However, there is a strong dependence of the peak temperature (at a given coverage) on sample weight. The explanation of this observation could arise from either interparticle diffusion control inside the bed or the degree of deviation from a differential bed which is caused by significant readsorption of desorbed species on the downstream catalyst. For either of these reasons the desorbed gas is retained inside the bed for longer times and hence the shift in the peak temperature. However, due to the high interstitial velocity of the carrier gas and the small bed length, the interparticle diffusion effect can be ignored. Thus the deviation from a differential bed caused by readsorption accounts for the peak temperature shift caused by samples

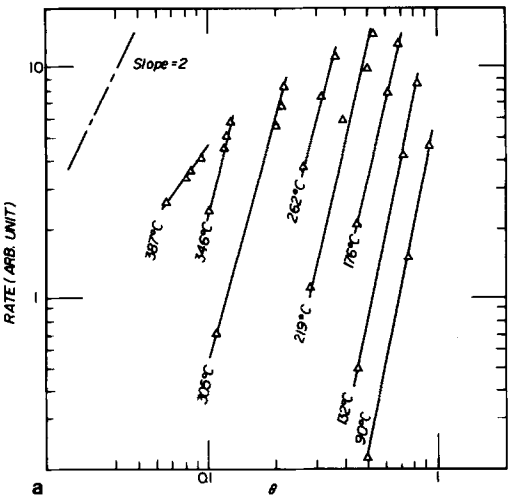


FIG. 7a. Desorption rate isotherms without readsorption correction for $H_2$ from 0.200 g $Ni/SiO_2$. The curves were obtained from spectra shown in Fig. 6a. Note that the slope is much higher than 2.

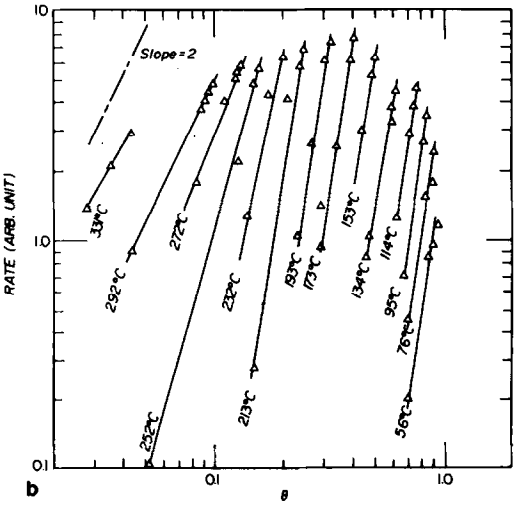


FIG. 7b. Desorption rate isotherms without readsorption correction for $H_2$ from 0.100 g $Ni/SiO_2$. The curves were obtained from spectra shown in Fig. 6d. Note that the slope is much higher than 2.

of different weight. This deviation becomes more serious as the sample weight increases.

Further confirmation of the readsorption effect during temperature-programmed desorption is established by the desorption rate isothermal analysis. Figures 7a and b show order plots on $\ln R$ vs $\ln \theta$ for the case of no readsorption. Figures 8a and b show plots of $\ln R$ vs $\ln(\theta/1 - \theta)$ to account for readsorption. In Figs. 7a and b lines of slope much higher than 2 are obtained. They have no physical meaning. On the other hand, Figs. 8a and b show a reaction order of 2 for the majority of the coverage range. The effects shown at very high and very low coverages are not understood. They may be due to different binding states or a different desorption mechanism.

To extract the coverage dependence of the kinetic parameters, Arrhenius plots of $\ln R$ vs $1/T$ at fixed coverage are made and illustrated in Figs. 9 and 10 for a catalyst weight of 0.100 and 0.200 g, respectively. The results show that the activation energy at low coverage is constant. Above some critical coverage the activation energy decreases with increasing coverage.

The coverage dependence of the desorption activation energy has been obtained from samples of different weight. The results are shown in Fig. 11. The low and high coverage values of the energy are independent of sample weight. However, the greater the sample amount, the lower the critical coverage. This suggests that the activation energy may be constant throughout a substantial coverage range if the sample amount is small. Unfortunately, detection sensitivity precluded a detailed study for samples less than 0.022 g.

The present results from 0.100- and 0.200-g samples can be compared with the results obtained from single crystals by Christmann *et al.* (*4*). The activation energy at low coverage is 89 kJ/mole in the present results and is in excellent agreement with the value of ~91–97 kJ/mole

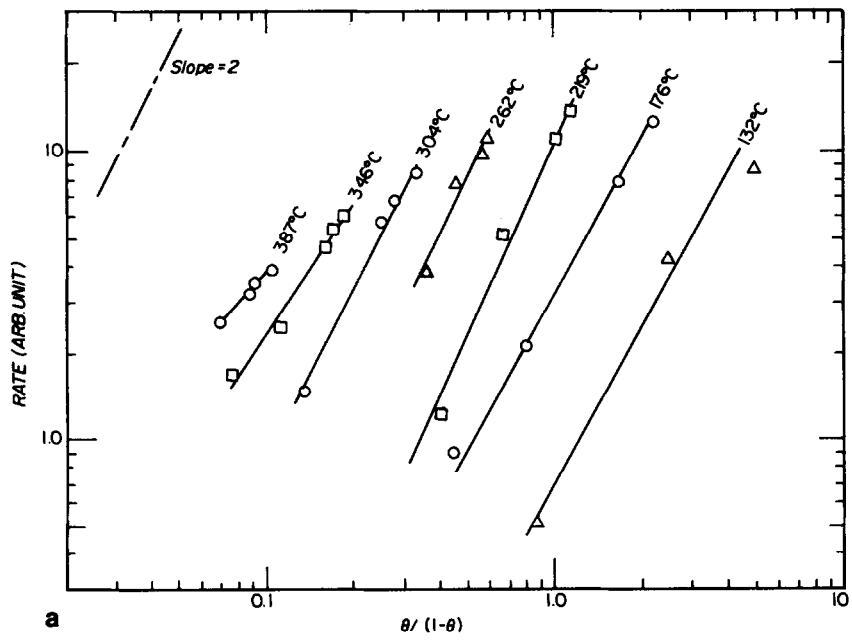


FIG. 8a. Desorption rate isotherms with readsorption correction for $H_2$ from 0.200 g $Ni/SiO_2$. The curves were obtained from the spectra shown in Fig. 6a. Note that the slope is 2 throughout a substantial range of coverage.

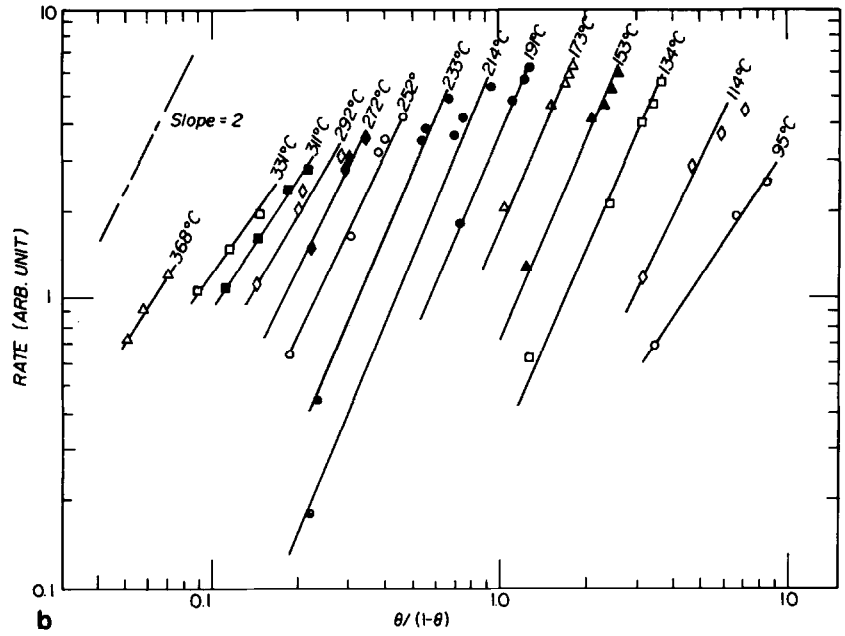


FIG. 8b. Desorption rate isotherms with readsorption correction for $H_2$ from 0.100 g $Ni/SiO_2$. The curves were obtained from the spectra shown in Fig. 6d. Note that the slope is 2 throughout a substantial range of coverage.

from their results. Above the critical coverage the activation energy is again constant at 54 kJ/mole. This is in excellent agreement with the data of Padberg and Smith (7) obtained at saturation coverage by a chromatographic technique and moment analysis.

Assuming the activation energy is con-

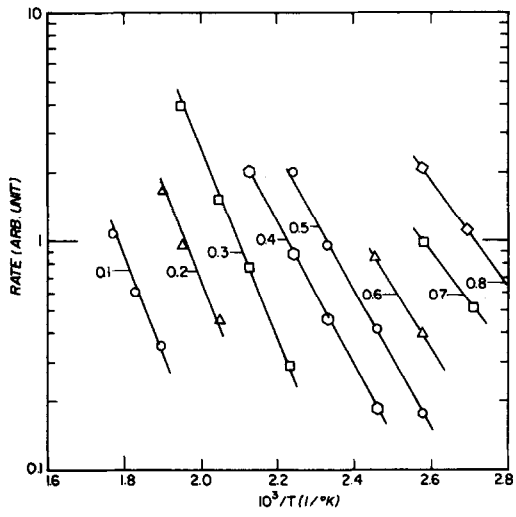


FIG. 9. The desorption energy determination of $H_2$ from 0.100 g $Ni/SiO_2$. The curves were obtained from Fig. 8b. The desorption energy decreases as coverage increases.

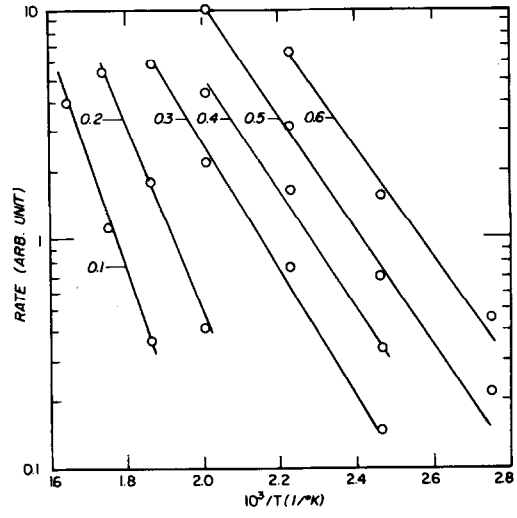


FIG. 10. The desorption energy determination of $H_2$ from 0.200 g $Ni/SiO_2$. The curves were obtained from Fig. 8a. The desorption energy decreases as coverage increases.

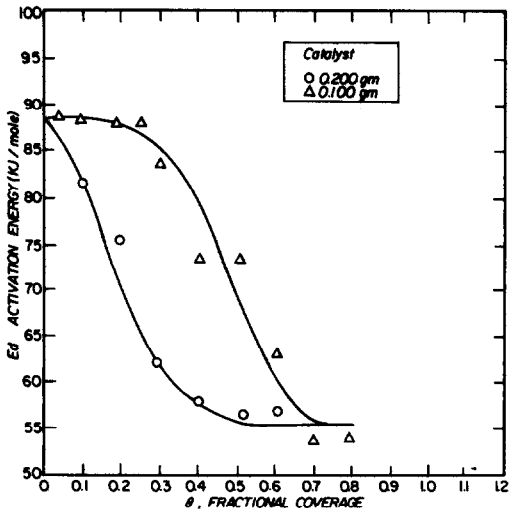


FIG. 11. The coverage dependence of the desorption energy for $H_2$ from 0.200 and 0.100 g $Ni/SiO_2$. Note that the 0.100-g sample has a higher critical coverage at which the desorption energy begins to decrease.

stant throughout a narrow range of experimental coverages, a direct comparison of the kinetic parameters from samples of different particle sizes and weights can be made by a characteristic plot analysis. Recall that this single-point analysis requires a measurement of the peak temperature and the coverage at this temperature at different initial coverages of hydrogen. A variation in the particle size by a factor of 10 introduces a pressure drop difference across the two beds of ~0.12 atm. We estimate that this pressure drop causes less than a 5% error in either the peak temperature or the coverage at this temperature. Therefore, a reliable test for intraparticle diffusional effects can be made by varying the particle size as we have done. Figure 12 shows the characteristic plot based on Eq. (15b) for 0.100-g samples of particle size 25 and 225 $\mu$m. Two lines of equal slope are observed. The activation energy given by the slope is ~67–71 kJ/mole which is small compared to the low coverage value obtained from the order plot analysis. However, the agreement in the activation energy confirms the absence of pore diffusion control. The smaller value arises from the fact that the activation energy is not constant over the coverage range (see Fig. 11) and thus an "average" value is obtained. Results for samples of different weight are also illustrated in Fig. 12. Lines of increasing slopes for decreasing sample weight are observed. The activation energy obtained from the 0.022-g sample has a value of ~79–83 kJ/mole, which is very close to the low coverage value obtained from the order plot. This clearly suggests that the activation energy is constant throughout a substantial range of coverage for this weight of sample. The agreement between the supported catalyst and its unsupported analog is again demonstrated.

## DISCUSSION

Pulsed chemisorption results have shown that the adsorption of hydrogen on the supported nickel catalyst is nonactivated and dissociative. The metal surface area obtained is in good agreement with static chemisorption results.

In the modeling of surface reaction mechanisms over supported catalysts there has

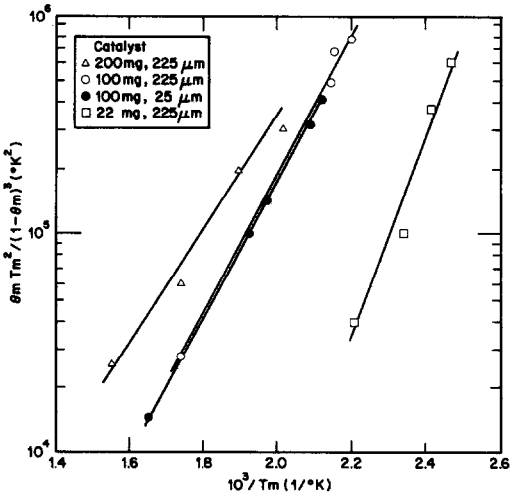


FIG. 12. Characteristic plot for $H_2$ desorption from $Ni/SiO^2$ with samples of different weight and different particle size. Note that the line for sample of weight 22 mg has a slope of ~81 kJ/mole.

been a growing appeal for considering the kinetic parameters determined from surface science studies in the modeling process. For example, Vannice (*26, 27*) has found an interesting relationship between the binding energy of carbon monoxide determined from single-crystal experiments and the turnover frequency for methane production over the supported Group VIII metals. The value of the initial sticking coefficient of a gas on a supported metal catalyst might, therefore, be of some importance.

Figure 3 shows that the amount adsorbed versus the number of hydrogen pulses is linear over a rather large range of pulses. This plot is identical to the amount adsorbed versus exposure results typically obtained from single-crystal studies. There the slope is directly related to the initial sticking coefficient of the adsorbate. The correspondence to the supported catalyst case, however, is not as direct. We obtain an initial slope of $1.5 \times 10^{13}$ molecules/cm$^2$ pulse and suggest that one may reasonably relate this result to the initial sticking coefficient of hydrogen on the supported nickel catalyst by the following considerations. Adsorption appears to be uniform on the basis of the surface area results. We imagine a catalyst bed composed of "monatomic" layers of nickel atoms. That is, the volume of the catalyst bed is divided into differential control volumes ($\sim 1$–$5 \times 10^7$ for a 5-mm bed) each of which contains one "monatomic" layer of nickel atoms. Therefore, the effective contact time for a gas molecule above each layer is $\sim 2$–$10 \times 10^{-8}$ times the actual contact time of the gas with the packed bed. The effective exposure is 1.9 Langmuir/pulse (1 Langmuir = $10^{-6}$ Torr · sec) which yields a value of $\sim 0.01$–$0.04$ for the initial sticking coefficient. Christmann *et al.* report (*4*) an average value of 0.25 on the three low-index planes of nickel but also find the adsorption to be $(1 - \theta)$. Other reports (*5, 6, 25*) give values that range from 0.04 to 0.1. Our result seems to be reasonable and furthermore provides a conceptual picture of the physical discrepancy between a packed bed of supported catalyst and a well-defined metal surface.

Transport effects must always be considered in evaluating data from adsorption–desorption studies of the type reported here. According to the criteria suggested by Weisz and Prater (*28*) and Ibok and Ollis (*29*), particles of size smaller than 500 $\mu$m will not have an appreciable intraparticle diffusion gradient. We have demonstrated this experimentally by observing no peak temperature shift when using samples of different particle size. The absence of external mass transfer control was also confirmed experimentally. The resistance to external mass transfer is inversely proportional to the fluid phase velocity (*30*) and thus if external mass transfer is controlling, the adsorption rate would be proportional to the carrier gas flow rate. This was shown not to be the case.

Although transport effects could be ruled out for our experimental system, the factor of readsorption could not. This has led to a semiquantitative conclusion to explain the variation in the activation energy of desorption of hydrogen as a function of its coverage. In comparing our data with the single-crystal (*4–6*) and supported nickel (*7, 21*) results of the activation energy and the heat of adsorption (the activation energy for adsorption was determined to be zero), respectively, the low coverage and high coverage values were in excellent agreement. The critical coverage at which the activation energy starts to decrease was found to be related to the sample weight (bed length).

The possibility of readsorption has not received much attention in the evaluation of TPD data from a flow system at atmospheric pressure. Our analysis has assumed free readsorption (equilibrium). When this is the case a rough correlation between the peak temperature at a fixed coverage as a function of bed length may be obtained from our data. The result for $L_1 > L_2$ is

$$T_{M_2}^{-1} = T_{M_1}^{-1} + \alpha \frac{L_1}{L_2},$$

where $L$ is the bed length and the peak temperature is in degrees Kelvin. For hydrogen desorption from nickel, $\alpha = 5.5 \times 10^{-5}$ and this equation is valid for bed lengths greater than 0.1 mm. We suggest that a similar correlation should exist for other gas–metal systems because the shift in peak temperature should be independent of the adsorption or desorption kinetics, although the value of $\alpha$ may be different.

Finally, in conclusion, we also found that analysis of the order plots corrected for readsorption gave desorption preexponentials that varied with coverage. The sympathetic variation in the activation energy with the preexponent is known as the compensation effect and has been reported before for many gas–solid systems (*17, 18, 31–33*). We, as others, can offer no interpretation of this phenomena.

## ACKNOWLEDGMENTS

We would like to acknowledge the courtesy of Dr. J. L. Carter for supplying the catalyst used in this work. Also, we would like to thank Mr. A. Efraimson and Mr. R. Korbler for technical assistance in building equipment.

## REFERENCES

1. Cvetanović, R. J., and Amenomiya, Y., "Advances in Catalysis and Related Subjects," Vol. 17, p. 102. Academic Press, New York/London, 1967.
2. Komers, R., Amenomiya, Y., and Cvetanović, R. J., *J. Catal.* **15,** 293 (1969).
3. For example, Zagli, E., Falconer, J. L., and Keenan, C. A., *J. Catal.* **56,** 453 (1979).
4. Christmann, K., Schober, O., Ertl, G., and Neumann, M., *J. Chem. Phys.* **60,** 4528 (1974).
5. Lapujoulade, J., and Neil, K. S., *Surf. Sci.* **35,** 288 (1973).
6. Lapujoulade, J., and Neil, K. S., *J. Chem. Phys.* **57,** 3535 (1972).
7. Padberg, G., and Smith, J. M., *J. Catal.* **12,** 172 (1968).
8. Freel, J., *J. Catal.* **25,** 139, 149 (1972).
9. Hausen, A., and Gruber, H. L., *J. Catal.* **20,** 97 (1971).
10. Gasiev, G. A., Filinovskii, V. Yu., and Yanovskii, M. I., *Kinet. Katal.* **4,** 688 (1963).
11. Hattoti, T., and Murakami, Y., *J. Catal.* **10,** 114, 123 (1968).
12. Redhead, P. A., *Vacuum* **12,** 203 (1962).
13. Ehrlich, G., *in* "Advances in Catalysis and Related Subjects," Vol. 14, p. 255. Academic Press, New York/London, 1963.
14. Falconer, J. L., and Madix, R. J., *J. Catal.* **48,** 262 (1977).
15. Christmann, K., Ertl, G., and Pignet, T., *Surf. Sci.* **54,** 365 (1976).
16. Falconer, J. L., and Madix, R. J., *Bull. Amer. Phys. Soc.* **21,** 935 (1976).
17. Schwarz, J. A., *Surf. Sci.* **87,** 525 (1979).
18. Schwarz, J. A., and Keleman, S. R., *Surf. Sci.* **87,** 510 (1979).
19. Konvalinka, J. A., Scholten, J. J. F., and Rasser, J. C., *J. Catal.* **48,** 365 (1977).
20. Johnson, S., and Madix, R. J., *Surf. Sci.*, in press.
21. Schuit, G. C. A., and Van Reijen, L. L., *in* "Advances in Catalysis and Related Subjects," Vol. 10, p. 242. Academic Press, New York/London, 1958.
22. See, for example, Falconer, J. L., and Wise, H., *J. Catal.* **43,** 220 (1976) and Lee, P. I., Masters thesis, Syracuse University, 1981.
23. Bartholomew, C. H., and Pannell, R. B., *J. Catal.* **65,** 390 (1980).
24. O'Neill, C. E., Thesis, Columbia University, 1961.
25. Madix, R. J., Ertl, G., and Christmann, K., *J. Chem. Phys.* **62,** 38 (1979).
26. Vannice, M. A., *J. Catal.* **44,** 152 (1976).
27. Vannice, M. A., *J. Catal.* **50,** 228 (1977).
28. Weisz, P. B., and Prater, C. D., *in* "Advances in Catalysis and Related Subjects," Vol. 6, p. 143. Academic Press, New York/London, 1954.
29. Ibok, E. E., and Ollis, D. F., *J. Catal.* **66,** 391 (1980).
30. Satterfield, C. N., "Mass Transfer in Heterogeneous Catalysis," Vol. 86. MIT Press, Cambridge, Mass., 1970.
31. Christmann, K., and Ertl, G., *Surf. Sci.* **60,** 365 (1976).
32. Taylor, J. L., and Weinberg, W. H., *Surf. Sci.* **40,** 37 (1979).
33. Bauer, E., Bonczek, F., Poppa, H., and Todd, G., *Surf. Sci.* **53,** 87 (1975).